RESEARCH REPORT

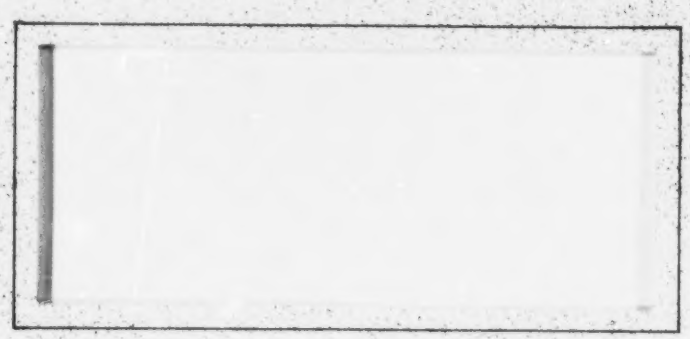

Welding Institute of Canada
Institut de Soudage du Canada

VISCOSITY EFFECTS IN SELECTED FLUX CORED ARC WELDING CONSUMABLES

by

Professor K. Leewis

Formerly Technical University of Nova Scotia

Now Welding Institute of Canada

April 1988

This work was funded by the Federal Panel on Energy R & D (PERD)

9161

DSS File Number:	38ST.23440-6-0161
DSS Contract Serial Number:	23440-6-9161/01ST
CANMET Scientific Authority:	Dr. J.E.M. Braid

62 pp

MICROMEDIA

TABLE OF CONTENTS

		Page
Abstract		(i)
List of Figures		(ii)
List of Tables		(iii)
Purpose		1
Introduction	a) Viscosity	2
	b) Surface Tension	4
Method		12
Results	a) Analysis	13
	b) Surface Tension	13
	c) Viscosity	17
Discussion	a) Viscosity	18
Conclusions		22
Recommendations		22
Acknowledgements		22
References		23
Appendix A -	Viscosity Data and Fusion Temperatures	24

ABSTRACT

Rutile flux cored welding consumables are preferred by welders. In order to understand why they perform better than basic and acid fluxes, the melting points and viscosities of a selected set of model fluxes were measured at elevated temperatures. The large change in viscosity was confirmed with these melts and also located in previous literature. This previously unreported ten fold jump in viscosity for rutile slags suggests that their preferred operation was due to the natural formation of precipitates on cooling and the resulting increases in viscosity and silicate cooling.

Les fil fourrés dont le flux est de type rutile sont ceux que les soudeurs préfèrent. Afin de mettre en évidence pourquoi ces fils se comportent mieux que ceux de type basique ou de type acide, les températures de fusion et les viscosités d'un groupe sélectionné de flux-types ont été measurées à hautes températures. Les grandes variations de viscosité de ces flux déjà rapportées dans des articles précédents, ont été confirmées par ces fusions. La chute de la viscosité par un coefficient 10 des flux rutiles, non rapportée jusqu'à présent, suggère que leur utilisation préférentielle provient de la formation naturelle de précipités lors due refroidissment ce quie crée une augmentation de la viscosité et de l'activité des silicates.

LIST OF FIGURES

Figure		Page
1	Correlation between A and B for oxide, silicate and alumino silicate melts (5).	5
2	Pinhey's Flux 10% TiO_2 (6).	6
3	Viscosity of Blast Furnace Slag and of a $CaO-Al_2O_3$ (7).	7
4	Effect of temperature and the addition of alumina on the viscosity of mould fluxes (8).	8
5	Temperature dependence of viscosity for welding fluxes (10).	9
6	Induction furnace for the determination of Flux Melting Temperatures (4).	12

LIST OF TABLES

Table		Page
1.	Typical Flux and Slag Compositions (FCAW) (3).	3
2.	Chemical Analysis of Industrial FCAW Consumable Fluxes.	15
3.	Activation Energies for Viscosity.	16
4.	Electrode Performance and Operator Appeal (1).	20

PURPOSE

In two recent reports, Bala (1) and Dorling (2) evaluated a range of FCAW consumables designed to join HSLA steels such as Stelco's 350WT and Algoma's LT60 that will see Arctic service. Basic, rutile and metal cored consumables were deposited and the pertinent mechanical properties obtained. What stood out, however, was the easier operation of the rutile based consumables. These all were rated much more acceptable than the metal core. The worst performers were the basic wires. The physical properties of the fluxes were thought to play a significant role in controlling the weld profile and transfer characteristics. Welds failed on poor profile alone, and difficult manipulation ensure that these consumables would not make it into the field.

The purpose of this contract was to obtain and analyze samples of the fluxes. The melting temperature and viscosity would be measured using both the extracted raw fluxes and also the slags after welding. These physical properties would then be used to determine a mechanism to explain the better performance of the rutile consumables.

INTRODUCTION

Flux cored arc welding (FCAW) appears extremely appropriate for the repair and fabrication of offshore structures. FCAW has the advantage of improving the weld metal chemistry control and with gas shielding, the possibility of a tougher mechanical performance. The essentially infinite length of the wire consumable reduces the chances of slag entrapment, porosity and crater-cracking.

The viscosity and surface tension of slags is controlled by chemistry, the composition of the various elements in the slags, and the resulting bonding in the three dimensional network systems. Welding fluxes fall into four different classes depending on the main ingredients:

i)	Titania	TiO_2-SiO_2
ii)	Lime Titania	CaO-TiO_2-SiO_2
iii)	Lime	$CaCO_3$-SiO_2-CaF_2
iv)	Basic	TiO_2-SiO_2-MnO

Performance can be greatly affected by impurities and these change depending on the geological origin of the raw materials. Jackson (3) provided a good review and also noted that there is a large variance in melting points of titania based fluxes with many melting above 1475°C, the melting point of most carbon steels (Table 1). There was also a change in the flux composition after welding with many of the alloying elements leaving the flux, hence, the increase in lime, slica and alumina. Since few fluxes use aluminum metal as a deoxident, it is possible to use alumina as an indicator of flux volume before and after welding. Therefore in most cases, the slag is usually half the weight of the original flux, with iron and maganese being transferred to the weld pool.

Viscosity

A recent review of titania welding systems (4) showed that there was a general lack of published data, especially for viscosity and surface tension

TABLE 1 **Typical Flux and Slag Compositions of the Four Types of Self-Shielded Flux-Cored Electrodes, %[a]**

Compound or element	*Type 1—fluorspar-aluminum*		*Type 2—fluorspar-titania*		*Type 3—fluorspar-lime-titania*		*Type 4—fluorspar-lime*	
	Flux	*Slag*	*Flux*	*Slag*	*Flux*	*Slag*	*Flux*	*Slag*
SiO_2	0.5	...	3.6	0.2	4.2	1.8	6.9	0.2
Al	15.4	...	1.9	...	1.4	...	...	...
Al_2O_3	...	11.8	...	6.5	...	6.0	0.6	12.8
TiO_2	...	...	20.6	27.0	14.7	33.5	1.2	2.3
CaO	...	...	...	...	4.0	...	3.2	4.1
MgO	12.6	9.2	4.5	4.5	2.2	6.0	...	0.9
K_2O	0.4	...	0.6	1.8	...	...	...	...
Na_2O	0.2	...	0.1	1.0	...	...	0.6	0.9
C	1.2	...	0.6	...	0.6	...	0.3	...
CO_2	0.4	...	0.6	...	2.1	...	1.3	...
Fe	4.0	...	50.0	...	50.5	...	58.0	...
Mn	3.0	...	4.5	...	2.0	...	7.9	...
Ni	...	...	...	...	2.4	...	...	...
CaF_2	63.5	76.1	22.0	53.0	15.3	47.5	22.0	73.7
MnO_2	...	0.4	...	1.1	...	2.8	...	0.7
Fe_2O_3	...	2.5	...	1.9	...	3.6	...	3.0
AWS classification[1]	E70T-4 E60T-7		E70T-3		E70T-6		E70T-5	

values. Since that time, a new model designed to predict the viscosity of continuous casting mold fluxes has been proposed by Urbain (5). Based on a molecular description of the network in these oxide electrolytes and using some previously developed viscosity data he was able to express viscosity as:

$$\mu = A.T. \exp (1000B/T)$$

where A: is a function of the mass; the energy level of a potential well (E_w); the volume; and the molar entropy of hole formation (Sr).

and B: is a function of Ew and Hv, the molar enthalpy of hole formation.

His regression to characterize A and B is shown in Figure 1. These estimates save considerable expense and time but assume a homogeneous liquid. Pinhey (6), however, discovered an anomily in one titanate system. In cooling a lead titania compound precipitated, changing the chemistry of the flux, and caused a tenfold increase in viscosity at that temperature. The activation energy for viscosity due to a higher silica fraction increased dramatically, i.e. a much higer viscosity (Figure 2). Another search through the literature indicated that this change in slope (activation energy for viscosity) has been previously reported but the two slopes were forced to intersect at a given temperature (7) (Figure 3). Turkdogan (8) provided an excellent review and also the first indication that there could be a dramatic change in the viscosity of mold fluxes with temperature (Figure 4). The lack of data suggested that it was just a freezing temperature phemonenon. Elliott (9) reported viscosity increases with the volume fraction of solids present. Before Pinhey, these two concepts had never before been blended. Limited data on welding fluxes had been reported by workers at the Welding Institute (10, 11). Davis (10) results are shown in Figure 5. The recalculated plots are found in Appendix A were the slope is proportional to the activation energy.

Surface Tension

Because of the experimental difficulties and the lack of data there are few

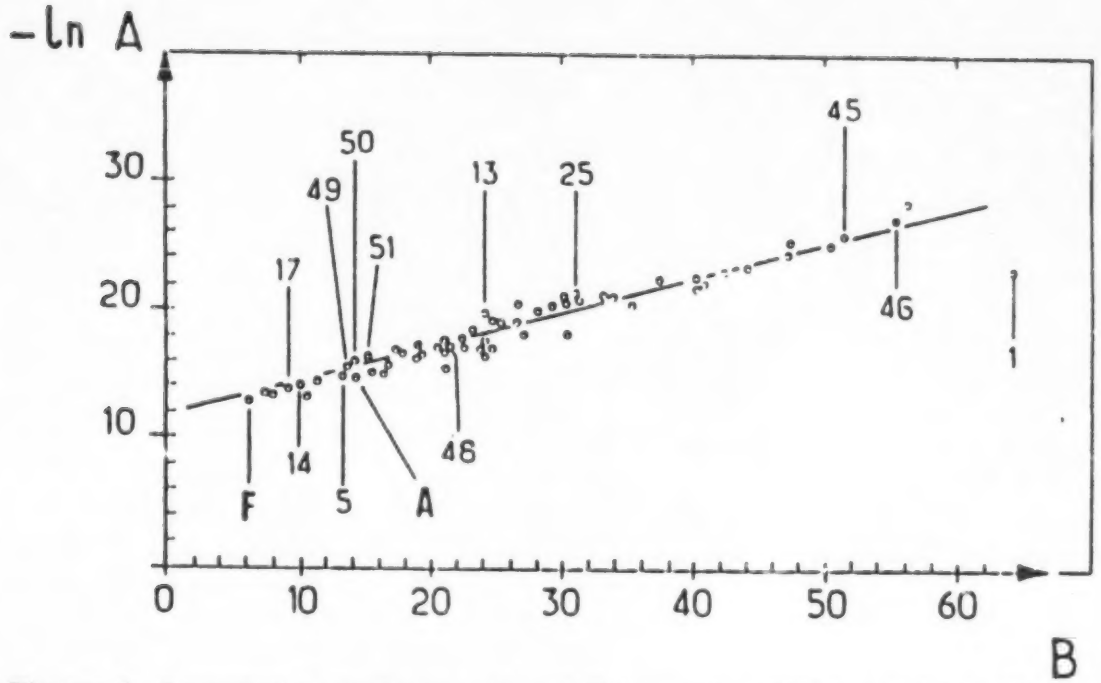

Figure 1. Correlation between *A* and *B* (equation (6)) for oxide, silicate and alumino-silicate melts. Melt compositions are identified by numbers corresponding to the entries of table 1 in [5]). F is for liquid FeO_x and A for liquid alumina

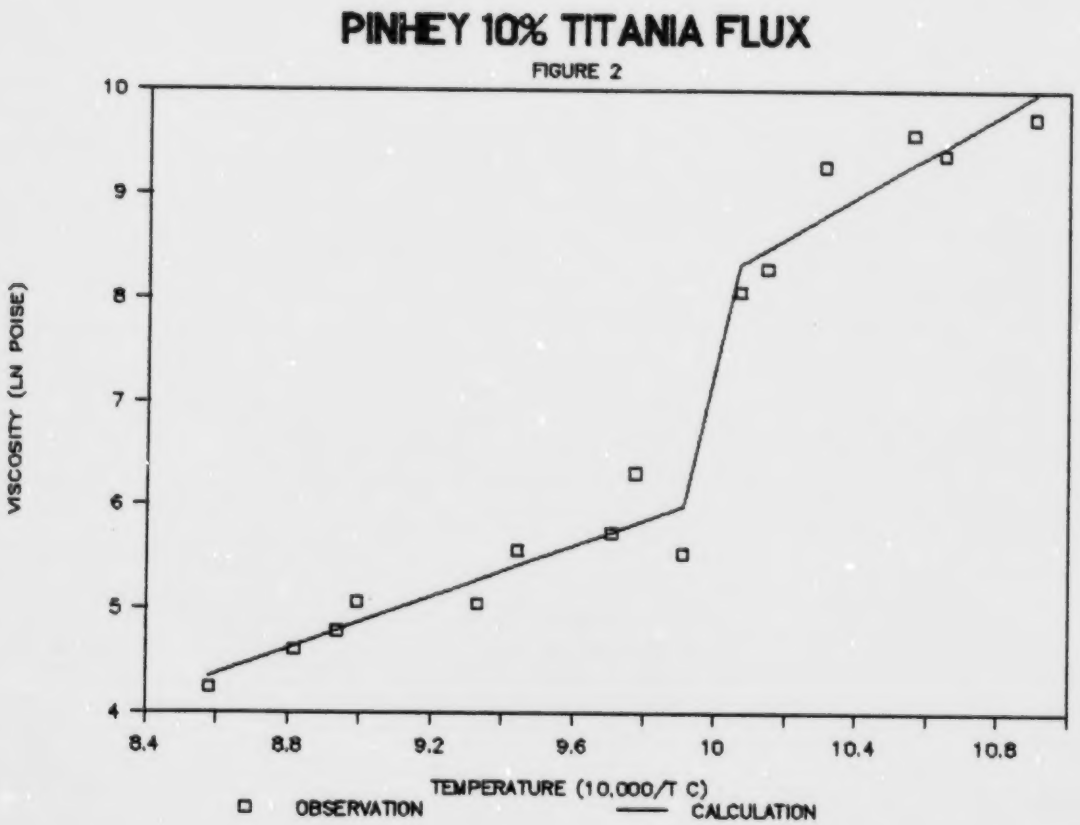
PINHEY 10% TITANIA FLUX
FIGURE 2
VISCOSITY (LN POISE)
10
9
8
7
6
5
4
8.4
8.8
9.2
9.6
10
10.4
10.8
TEMPERATURE (10,000/T C)
OBSERVATION
CALCULATION

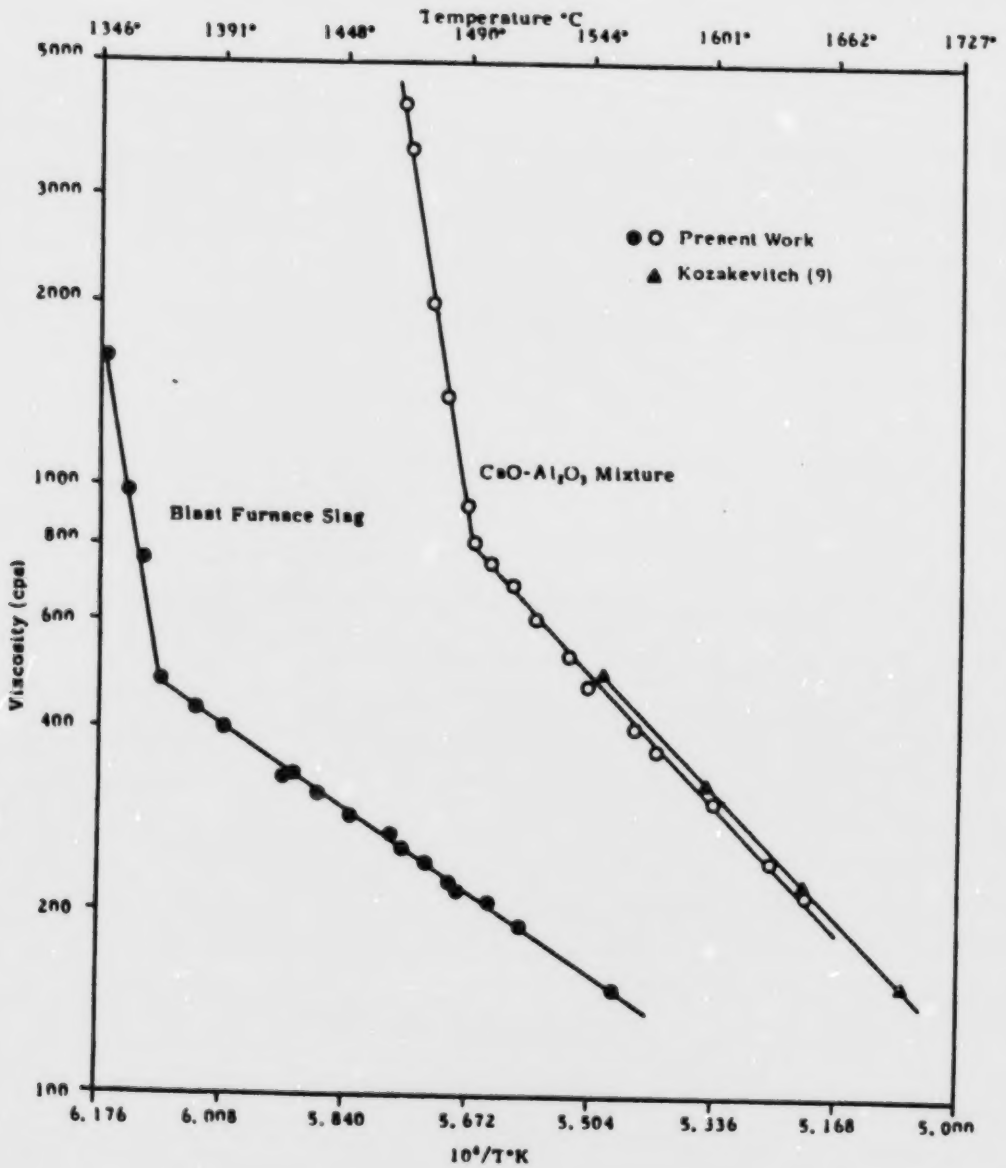

Figure 3 Viscosity of a blast furnace slag and of a $CaO\text{-}Al_2O_3$ mixture.

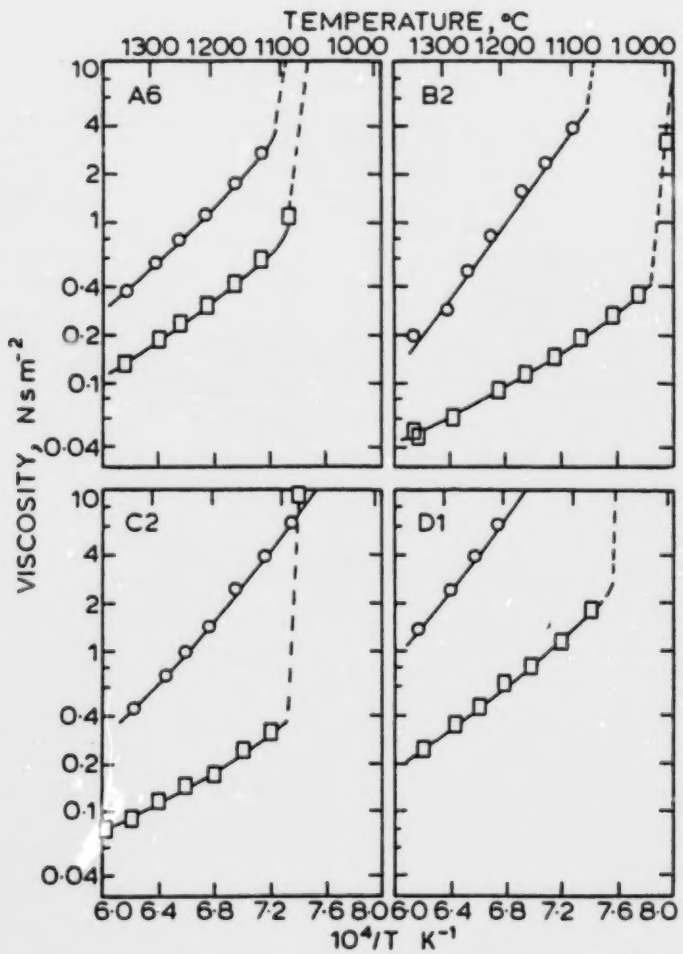

Figure 4 **Effect of temperature and addition of alumina on the viscosity of mould fluxes: (□) no Al_2O_3 added; (○) 25%Al_2O_3 added.**

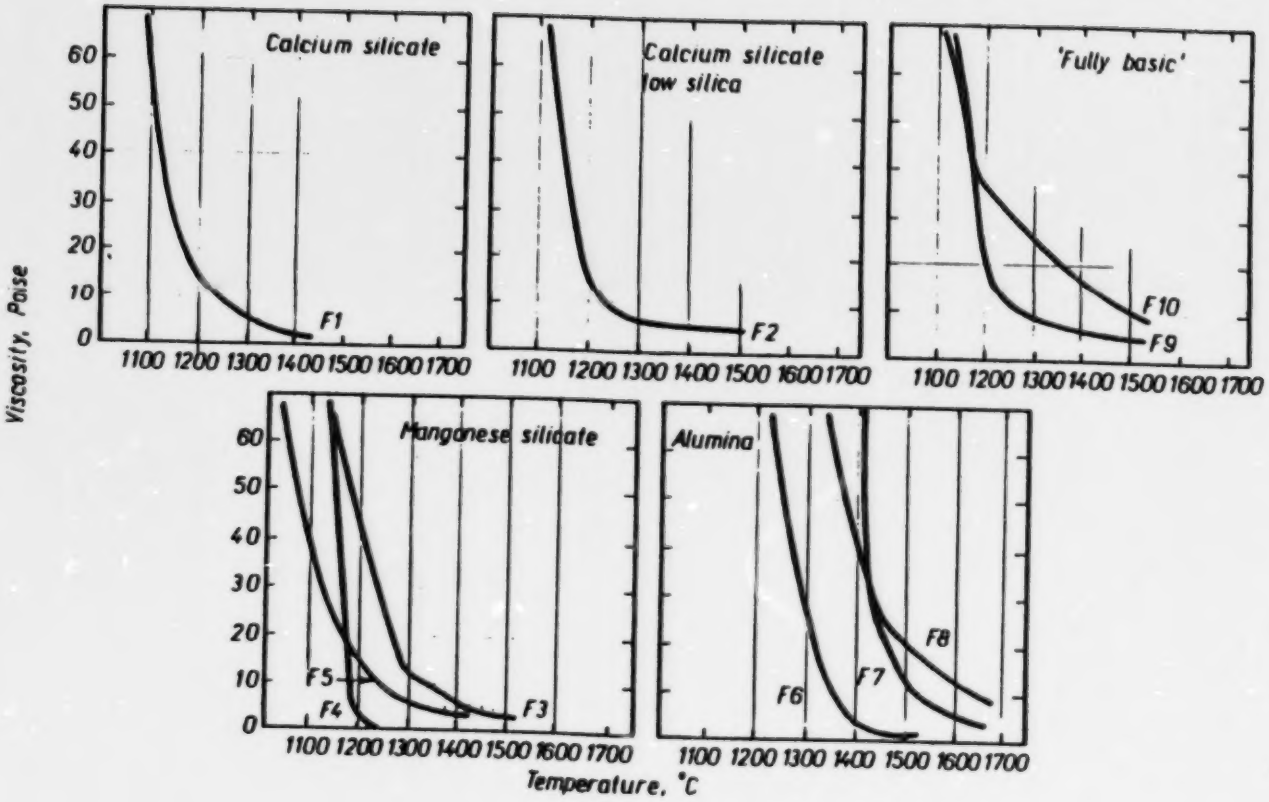

Figure 5 Temperature dependence of viscosity for welding fluxes (10).

measurements of interfacial tension for iron alloys with fluxes, especially with welding fluxes. Turkdogan (8), again provides a useful review and the majority of the data was collected by Mills (11). The more recent report for DREA (4) attempted to measure the surface tension of titania fluxes. Experimental problems due mainly to severe refractory corrosion and temperatures at and above the melting point of steel, suggested that the sessile droplet technique was not suitable to properly rank the surface tension of the fluxes. The literature review pointed out that the key parameter to obtain was the metal interfacial tension. High surface tension was only possible by the strict control of oxygen and other surface active elements such as sulphur. Extremely pure iron has a surface tension exceeding 1800 mNm^{-1} (8). The presence of oxide fluxes prevented the surface tension to rise above 1,000 mNm^{-1} and generally ensured that the interfacial tension remained below 600 mNm^{-1}. Out of position welding requires a high surface tension to support the weight of the liquid weld pool. This suggests that GMAW systems inherently have a better potential to improve out of position welding than flux containing systems.

The values reported in the literature were obtained in the absence of an electrical field. Both viscosity and surface tension are composition dependent. Imposed electrical fields have been used to desulphurize and deoxidize molten melts and this phenomena in purely ionic electrolytes also provides the basis for the operation of oxygen potential cells. Viscosity should be relatively independent of the imposed voltage and current. However, surface tension is highly sensitive. This interdependence of surface tension and applied potential is termed the electro-capilliary pheomena and must always be present in welding systems. As yet, very little experimental data is available and modelling ignores the phenomena.

Essentially, fluxes are continously being improved, however, some observations are possible based on this report. The rutile FCAW consumables seem to give a better weld profile and have a more stable operating envelope than the basic consumables. Conversely, the weld metal toughness properties seem much better with the basic wires. The total oxygen levels are considerably different, welds using basic fluxes had the lowest concentration

averaging 550 ppm, rutile at 800 ppm, and the metal core the highest at 900 ppm. These are much higher than generally desired for best toughness at low temperatures and the authors suggest that 250 ppm would be the desirable concentration to ensure sufficient toughness by the promotion of acicular ferrite (even at the preaustenite grain boundaries) and to avoid inclusions >1.0 m. These larger inclusions just in front of the fatigue crack can lead to pop-ins and reduced toughnesses. Bala's report did not confirm that the total oxygen had a significant effect on microstructure as each of the three classifications had similar Cvn, CTOD and acicular ferrite levels at the above concentrations: basic 550 ppm, rutile 800 ppm, and metal core at 900 ppm. The results had a larger scatter suggesting more control was warranted. The regression shows that there is no Cvn versus CTOD correlation for this work. Only the composition was correlated for toughness while microstructure and stress concentrations were not considered. The following conclusions were offered to increase CTOD toughness:

1) reduced size, volume fraction, and number of inclusions in each weld.

2) reduced grain boundary ferrite (the nucleation of this microstructure is associated with inclusions).

3) increasing the cleavage resistance of the grain boundary ferrite, i.e., add nickel, reduce inclusion size.

4) refining and increasing the acicular ferrite content especially at the preaustenite grain boundaries.

There are conflicting theories on how oxygen, usually as an inclusion, catalyses the acicular ferrite formation, however, all agree that a controlled level of oxygen in the weld pool is desired before solidification occurs. Oxygen control is achieved by minimizing sources in the gases and consumables, by ensuring that it is tightly bound to flux components and by the addition of deoxidants, i.e., Si to rare earth metals.

Basic oxides are used to ensure cleaner microstructures as they readily absorb alumina deoxidation products by forces such as surface tension. Interfacial tension between the metal and slags is higher with basic fluxes, as high as 1000 dynes. These very basic fluxes tend to behave as heterogeneous solid-liquid mixtures with inherently large interfacial tension gradients. Acid fluxes containing a large silica component tend to have interfacial tensions less than 400 dynes and a very homogeneous composition. The inferior operating behaviour, apparently the poor weld bead profile observed with most basic welding consumables, could be due to Marangoni effects caused by their heterogeneous nature. High interfacial tensions promote non-wetting behaviour and very large gradients result in a variable or "humpy" profiles. Rutile fluxes are homongeous, have strong oxygen bonding and as this work shows can form precipitates with large changes in the physical properties near the melting point. This change in structure to a liquid, acid flux apparently lowers the surface tension and causes the bead to flatten and blend into the parent metal without the excessive convex profile normal with higher interfacial tensions. This characteristic can explain the better subjective assessment rutile consumables received from the operators. Cleanliness or higher oxygen contents measured in the weld would be the result of the high silica content after precipitation and just before solidification. The high silica loads the interface with oxygen and this oxygen can be dragged into the weld pool by the strong liquid movement.

Method

The measurement techniques for viscosity, surface tension and extraction of the flux from the wire consumables have been described in detail in previous publications (4, 6). Briefly, the viscosity was measured by rotating a slip cast CaO-ZrO_2 cylinder, in the molten flux, at a variety of speeds. The torque as measured by the Brookfield viscometer was proportional to the viscosity after calibration with known fluids. The surface tension measurements were performed in an induction furnace (Figure 6). The cylindrical pellet of flux was placed on a lime stabilized zirconia disk and the chamber flushed with flowing Argon. The melting temperature was measured with a two colour optical pyrometer and the molten shapes photographed. The contact angle between the pellet and the disk was proportional to the surface tension.

The flux was extracted from the inside of the tubular consumable by winching the cored wire past a hardened point which peeled open the steel sheath. The metal slivers were removed before analysis. The slags after welding were crushed and the larger metallics removed by hand screening and picking. Both the fluxes (from inside the steel sheath) and the slags (after welding) were analyzed by standard wet chemical techniques.

The surface wetting was measured with actual fluxes. The viscosity measurements, however, were performed on model fluxes. The analysis of the extracted fluxes indicated a high proportion of iron and iron oxide. Both are highly corrosive to the zirconia and platinum crucibles available and, therefore, the iron was eliminated. Eutectic compositions in the $CaO TiO_2 SiO_2$ system was chosen to ensure the model fluxes were liquid at 1400°C.

Results

Analysis

The consumables received from CANMET and the analysis of these fluxes and slags are found in Table 2. Added for comparison are the rutile consumables designed to weld a high strength alloy, HY80. Comparison shows that the titania based fluxes contained between 30 and 40 wt% TiO_2 with the other major compound iron or iron oxide followed by silica and lime. The nickel in the fluxes was essentially absent in the slags suggesting a very efficient transfer into the weld metal. Using alumina as a tracer, roughly half of the manganese and silicon was transferred into the weld pool from the consumable flux.

Surface Tension

A great many measurements were taken of the welding angle of the slags and fluxes in the previous work (4). It was preferable to use a clean steel surface, accordingly an Argon + 5% H_2 atomsphere was used to ensure that oxygen was not absorbed by the iron surface. The melting temperatures of

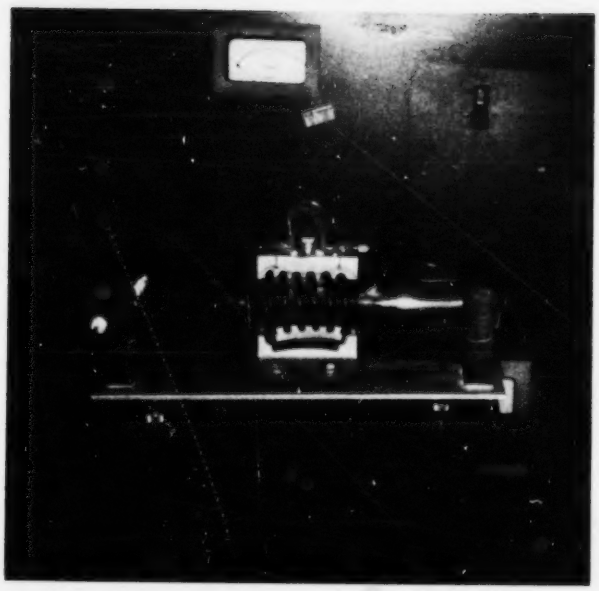

Figure 6. Induction furnace for the determination of Flux Melting Temeratures (4).

Chemical Analysis of Industrial FCAW Consumable Fluxes. TABLE 2

	FLUX/SLAG	TYPE	AWS ID	TiO2	SiO2	MnO	Fe+Fe2O3	Ni	Al2O3	CaO	MgO	Fe	Fe2O3	V-RATIO	TiO2/SiO
A	F	RUTILE	E81T1-Ni1	37.4	10.97	19.61	21.58								
	S			63	7.46	12.26	5.21	5.6	0.25	0.83	3.56		21.58	0.39	3.41
B	F	RUTILE	E91T1-K2	42.3	11.28	18.71	9.1	0.07	0.7	0.96	4.78		5.21	0.70	8.45
	S			59	7.75	12	10.82	9.6	0.24	0.62	3.29		9.1	0.34	3.75
C	F	RUTILE	E100T1-K3	47.1	13.35	14.8	4	0.19	0.71	0.86	4.12		10.82	0.59	7.62
	S			47.1	13.25	14.8	4	12.4	0.37	0.92	1.65	4	0	0.19	3.51
D	F	RUTILE+Al	E111T1-K3	30.7	11.02	25.8	13.21	12.4	0.37	0.92	1.65	4	0	0.19	3.55
	S			51.73	7.13	13.8	19.94	11.7	0.25	0.84	2.58		13.21	0.30	2.79
E	F	BASIC+Fe	E81T1-Ni2	0.18	8.58	4.33	63.5	N/A	0.78	1	3.68		19.94	0.59	7.26
	S			1.8	16.42	5.51	9.46	8.7	0.12	12.19	0.27		63.5	1.43	0.02
F	F	RUTILE+Fe	E4801T-9C	42.8	11.56	18.1	21.2	0.06	0.87	42.93	1.18		9.46	2.55	0.22
	S			49.5	7.87	12.9	4.29	0.025	4.57	0.6	0.14	21.2	0	0.05	3.70
G	F	METAL	E71T-C	0.14	11.29	9.26	80.4	0.002	7.34	0.6	0.27		4.29	0.05	6.29
	S			1.33	8.81	3.61	75.79	0.025	0.05	0.7	0.07	80.4	0	0.07	0.01
H	F	ACID+Fe	E71T-G	2.76	18.68	15.2	57.2	0.019	1.41	6.28	1.77		75.79	0.78	0.15
	S			2.76	18.68	15.2	57.2	0.045	1.53	3.05	1.17	0	57.2	0.21	0.15
I	F	METAL	E81T-G-Ni	0.89	15.15	6.77	66.83	0.045	1.53	3.05	1.17		57.2	0.21	0.15
	S				SLAGLESS			0.02	0.15	10.73	1.31	66.83	0	0.79	0.04

TUBULAR CONSUMEABLES :F
BEAD ON PLATE :S

Chemical Analysis of Industrial FCAW Consumable Fluxes.

TABLE 3

Activation Energies for Viscosity in Welding Fluxes

IDENT	CLASS	V	SLOPE	ACTIV'N ENERGY kcal/MOLE ave	LOW	HIGH	JUMP
D F1	CaOSiO2	M	16300.00	8.21			
D F2	CaOSiO2	M	10700.00	5.39	5.50	1.70	
D F3	MnSiO3	M	14600.00	7.35	6.90	?	X3.2
D F4	MnSiO3	L	80000.00	40.28			
D F5	MnSiO3	M	13700.00	6.90	6.30		X3.2
D F6	ALUMINA		28900.00	14.55			
D F7	ALUMINA		24600.00	12.39	11.10		X6.2
D F8	ALUMINA		13300.00	6.70			
D F9	BASIC	M	12300.00	6.19	8.40	3.60	X3.2
D F10	BASIC	H	8000.00	4.03			
EUT J	TITANATE	0.70	16700.00	8.41	5.50	?	X31
EUT L	TITANATE	0.60	33900.00	17.07			
EUT P	TITANATE	1.39	48800.00	24.57	25.20	?	JOINED
H/C LOW	TITANATE		42500.00	N/A	21.40	3.47	X6.2
H/C HI	TITANATE		66740.00	N/A	33.61	0.23	JOINED
H/C CT	CaOTiO2	1.00	19730.00	N/A	9.93	>1	JOINED

KEY
V = CaO/SiO2: LOW, MEDIUM, HIGH
HIGH = HIGH TEMP ACTIVATION ENERGY
LOW = LOW TEMP ACTIVATION ENERGY
JUMP = STEP INCREASE IN VISCOSITY

the fluxes were high and, in too many cases, the cylindrical pellet slid off the molten iron surface before melting. The high iron containing fluxes were too aggressive for aluminia or magnesia so zirconia substrata were used. The lack of data prevented intelligent interpretation of the wetting angles. In the end, only the melting point was felt to be concrete enough to report. The measured temperatures are reported in Appendix A in the appropriate tables.

The determination of the melting temperature was best illustrated by viewing the accompanying video. In the video, the obvious change from cylindrical to droplet shape was apparent and the corresponding temperature easily determined. The wetting angle of the samples was also apparent and can be seen in the video shots of the melted fluxes on the substrata at the end of that segment.

Further measurements would be best done using Professor Toguri's x-ray furnace at the University of Toronto. The use of fluoroscopy enables the metal shape to be viewed in a known slag-metal-gas system. With some ingenuity, it might also be possible to study electro capilliary effects as well.

Viscosity

It was originally planned to measure the viscosity of the actual fluxes in standard alumina crucibles. The extreme corrosivity of these systems suggested that an iron oxide free flux composition be chosen from the model CaO-TiO_2-SiO_2 phase diagram. The three low melting point eutectic compositions were weighed out, pressed into pellets and the melting points confirmed first. Viscosity experiments require experimental times exceeding three hours. Lime stabilized zirconia crucibles were slip cast and fired to the required diameter. Each flux was loaded in the crucible and melted in situ in a $MoSi_2$ furnace to which the Brookfield viscometer was adapted. The programable controller allowed the temperature to be adjusted in steps down from 1450°C and held until a stable viscosity reading was obtained. The results are tabulated in Appendix A.

The work of Davis et al (10) provided a useful reference, however, it was

only published as raw data. Similarly, plots of raw data for titania and other welding systems were reported by Turkdogan[8] and Jackson[3]. These were interpolated and the recalculated plots of ln vs $10^4/T$ are also found in Appendix A.

DISCUSSION

Viscosity

Pinhey was the first to report the ten fold increase in viscosity associated with the formation of $2PbO\text{-}TiO_2$ precipitates. The data found in Appendix 1 taken from several reviews was rearranged and plotted as ln η vs $10^4/T$. Since viscosity can be described by the following equation:

$$\eta = A \exp(-E/RT)$$

then the slope of the plot gives -E/R and the intercept A. The activation energies for selected systems are reported in Table 3. Pure SiO_2 has an activation energy of 580 kJ/mole at 1700°C and exceeds by a large margin the values reported in Table 4. Many of the systems gleened from literature have only an approximate composition or no values were reported. So it is difficult to relate the activation energies to the mole fraction of silica, the network forming component or any other constituent relationship. However, one may suggest that higher activation energies suggest higher silicate contents. Regressions were performed on selected systems. These are reported also in Table 4. The slope was considered -E/R but reviewing the plots, Figures A1 to A16 suggest that the regression does not always provide the best interpretation. Re-evaluation suggests that many of these systems have a high temperature and a lower temperature behaviour with separate slopes, hence separate structures present. Pinhey's work showed that precipitation of $2PbO\text{-}TiO_2$ left behind an extremely viscious, high slicia matrix. Unfortunately, these slags were all ground to 325 mesh and no metallography exists. There is no reason to think that this same phenomena of precipitation cannot occur especially since titania systems are known to form precipitates.

The recent DREA report (4), suggested that the formation of precipitates at a unique temperature lead to the jump in viscosity and the change in activation energy for these slag systems. The jump in viscosity was due to the "thickening" effect of the precipitates plus the increase in activation energy due to the much higher SiO_2 content of the liquid matrix. If this change occurs at the solidifying end of the weld pool then the sudden increase in viscosity would help to maintain the flatter profile. Simultaneously, the high silica liquid matrix would tend to make oxygen available to the weld pool, super-saturating the surface and enabling the weld profile to remain flat. If solidification occurred rapidly, then the increased oxygen concentrated at the slag metal surface could only just start to be swept into the pool with adverse effects. Quick metal solidification just after the formation of these slag precipitates would make for a flat weld profile with little chance for reoxidation. In this case, mechanical properties at low temperatures should not be adversely effected.

Only the rutile slags exhibited the decade increase in viscosity. Some of the basic and manganese silicate systems also exhibited this change but to a lesser degree. Table 4 was reported in Bala's work (1) and these subjective performance evaluations suggest that the rutile systems were preferred by the operator. Preference suggests flat bead profiles and a quickly solidifying flux are desired. This profile was probably the result of a titanate precipitation and a slag matrix chemistry change.

TABLE 4
Electrode Performance and Operator Appeal (1)

CLA T-75 Basic	- poor wash characteristics - hard to remove flux from corners - fair bit of spatter - arc not too stable - lots of undercutting - increased gas flow to 40 psi to supply adequate shielding.
Hobart Fabco 85 Basic	- undercutting - lots of spatter - porosity in radiographs - slag removal problems.
Esab Tubrod 15.00 Basic	- very bad spatter - poor performance - undercut
Hobart Fabco 806 Basic	- very peaky bead - no wash - lots of spatter - root pass not too good - backgouge showed defects in root.
Esab Tubrod 15.25 Basic	- some spatter - poor wash characteristics - fair performance.
Philips PZ 6140 Basic	- bad spatter - flux interference ahead of arc - undercut - DC straight polarity.
CLA Dual Shield II 80 Ni Rutile	- shielding gas set at 40 psi - good performance - minor spatter
MacKay 81 NiV Rutile	- 8 passes required due to higher voltage - performance satisfactory.
CLA Dual Shield II 70 Rutile	- good puddle control - some spatter - little bit of undercutting - gas shielding increased to 40 psi because of apparent pinholes.
Fabco 803 Rutile	- good performance - eash arc control - minor spatter.

TABLE 4 (Cont'd)
Electrode Performance and Operator Appeal(1)

Kobe DW-55L Rutile	- gas shielding increased to 45 psi - performance satisfactory
Hobart Fabcor 86 Metal Core	- Minimum spatter - good performance.
CLA Prototype Metal Core	- good performance - minimal spatter.
Esab Turbrod 14.00 Metal Core	- very poor performance - lots of spatter - poor wash characteristics - unstable arc.
Esab Tubrod 14.04 Metal Core	- DC straight polarity - good performance - a bit of spatter - some undercut.
Lincoln NR 203 NiD Metal Core	- very poor performance - lots of spatter - peaky bead, no wash - susceptible to slag entrapment - DC straight polarity.

CONCLUSIONS

The preferred operation of titania based FCAW consumables was due to their natural formation of precipitates on cooling.

RECOMMENDATIONS

1. Selected flux compositions should be chosen to correlate the viscosity dependence on temperature and microstructural behaviour.

2. A fluoroscope technique should be used to confirm the change in metal surface tension with the precipitation of titanate compounds from the model welding fluxes.

ACKNOWLEDGEMENT

The author would like to thank Drs Braid, North, Bala and Caley for their helpful discussions. This work would not have been possible without the help of Mr. Anil Rao, Mr. Paul Webster and Mr. Scott MacIntyre who's Bachelor theses provided the foundation for interpretation.

References

1. Bala, S.R. and Santur, S., EMR DSS Report 7-184-096/F, March 1986.

2. Dorling, D. et al, EMR DSS Report.

3. Jackson, C. E., WRI Bulletin No 190, Dec. 1973.

4. Leewis, K.G., DREA DSS 09SC97707-4-6146, July 1987.

5. Urban, G., "Viscosity Estimate of Slags", Steel Research 58 (1987), No.3, p.111.

6. Pinley, C., MASc Thesis, Technical University of N. S., 1987.

7. Handfield, G. and Charette, G.G., "Viscosity and Structure of Industrial High TiO_2 Slags", Can. Met. Quart., Vol.10, No.3 (1971), p.235.

8. Turkdogan, E.C., Physiochemical Properties of Molten Slags and Fluxes, The Metals Society, London, 1983, pp 478 - 484.

9. Elliott, J. F., 2nd Int. Symp. Metallurgical Slags and Fluxes, ed. H.A. Fine and D. R. Gaskell, TMS, AIME 1984, pp 45 - 60.

10. Davis, M.L.B. and Coe, F.R., Welding Institute 39/1977/M May 1977.

11. Mills, K.C., National Physical Laboratory Report, Chem 65, 1977, London, HMSO.

APPENDIX A
Viscosity Data and Fusion Temperatures

DAVIS' FLUX F1

FIG A.1

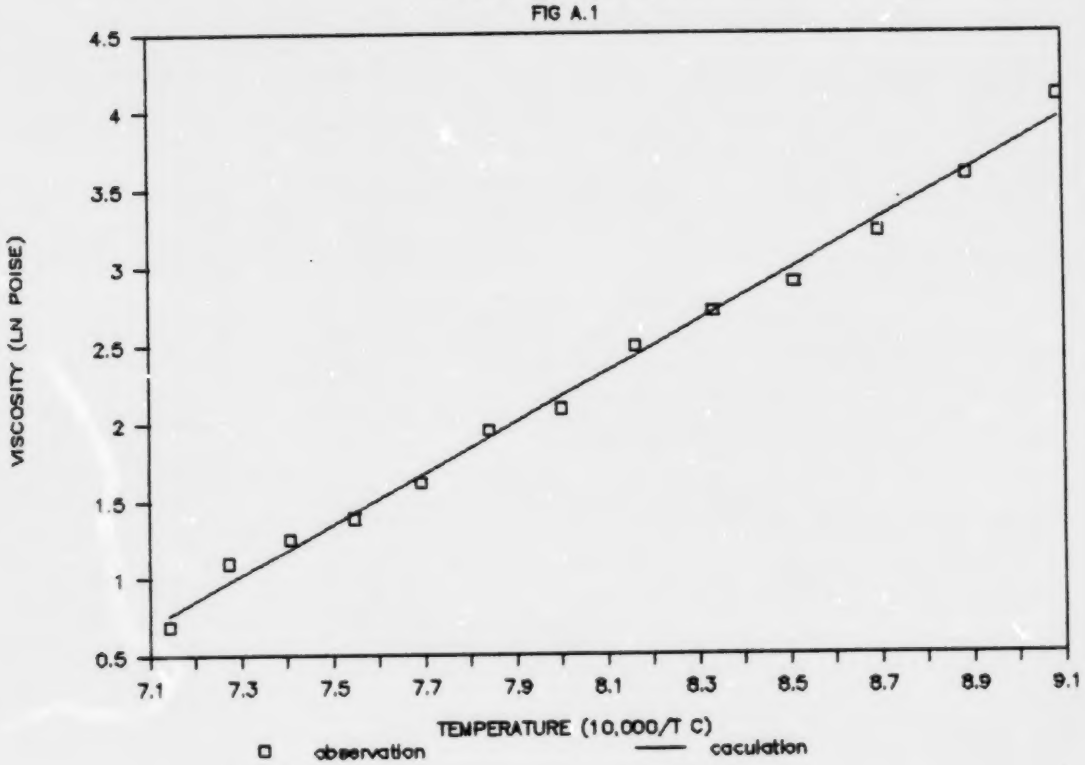

DAVIS' VISCOSITY F1

TABLE A.1

TEMP	POISE	10000/T	LN(POISE)	CALC LN VISC
1400.00	2.00	7.14	0.69	0.76
1375.00	3.00	7.27	1.10	0.97
1350.00	3.50	7.41	1.25	1.19
1325.00	4.00	7.55	1.39	1.42
1300.00	5.00	7.69	1.61	1.66
1275.00	7.00	7.84	1.95	1.90
1250.00	8.00	8.00	2.08	2.16
1225.00	12.00	8.16	2.48	2.43
1200.00	15.00	8.33	2.71	2.70
1175.00	18.00	8.51	2.89	2.99
1150.00	25.00	8.70	3.22	3.30
1125.00	36.00	8.89	3.58	3.61
1100.00	60.00	9.09	4.09	3.94

Regression Output:

Constant		-10.90
Std Err of Y Est		0.09
R Squared		0.99
No. of Observations		13.00
Degrees of Freedom		11.00
X Coefficient(s)	1.63	
Std Err of Coef.	0.04	

DAVIS' FLUX F2

FIG A.2

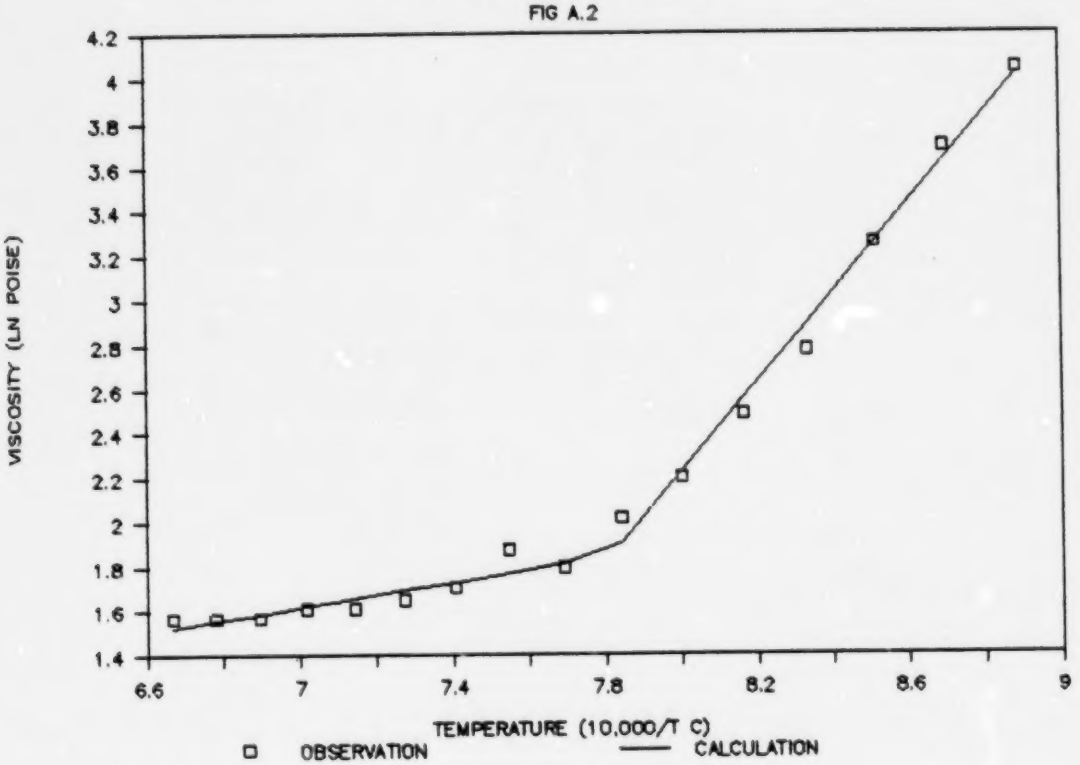

DAVIS' F2 SLAG

TABLE A.2

TEMP	POISE	10000/T	LN(VISC)	CALC LN VISC
1500	4.8	6.666666	1.568615	1.523547
1475	4.8	6.779661	1.568615	1.554965
1450	4.8	6.896551	1.568615	1.587466
1425	5	7.017543	1.609437	1.621107
1400	5	7.142857	1.609437	1.655950
1375	5.2	7.272727	1.648658	1.692059
1350	5.5	7.407407	1.704748	1.729506
1325	6.5	7.547169	1.871802	1.768367
1300	6	7.692307	1.791759	1.808721
1275	7.5	7.843137	2.014903	1.850659
1250	9	8	2.197224	1.894274
1225	12	8.163265	2.484906	1.939669
1200	16	8.333333	2.772588	1.986955
1175	26	8.510638	3.258096	2.036254
1150	40	8.695652	3.688879	2.087696
1125	57	8.888888	4.043051	2.141425

Regression Output:

Constant	-0.33008
Std Err of Y Est	0.051207
R Squared	0.805797
No. of Observations	9
Degrees of Freedom	7
X Coefficient(s)	0.278044
Std Err of Coef.	0.051591

Regression Output:

Constant	-13.9726
Std Err of Y Est	0.085603
R Squared	0.989589
No. of Observations	7
Degrees of Freedom	5
X Coefficient(s)	2.023924
Std Err of Coef.	0.092838

DAVIS' FLUX F3

FIG A.3

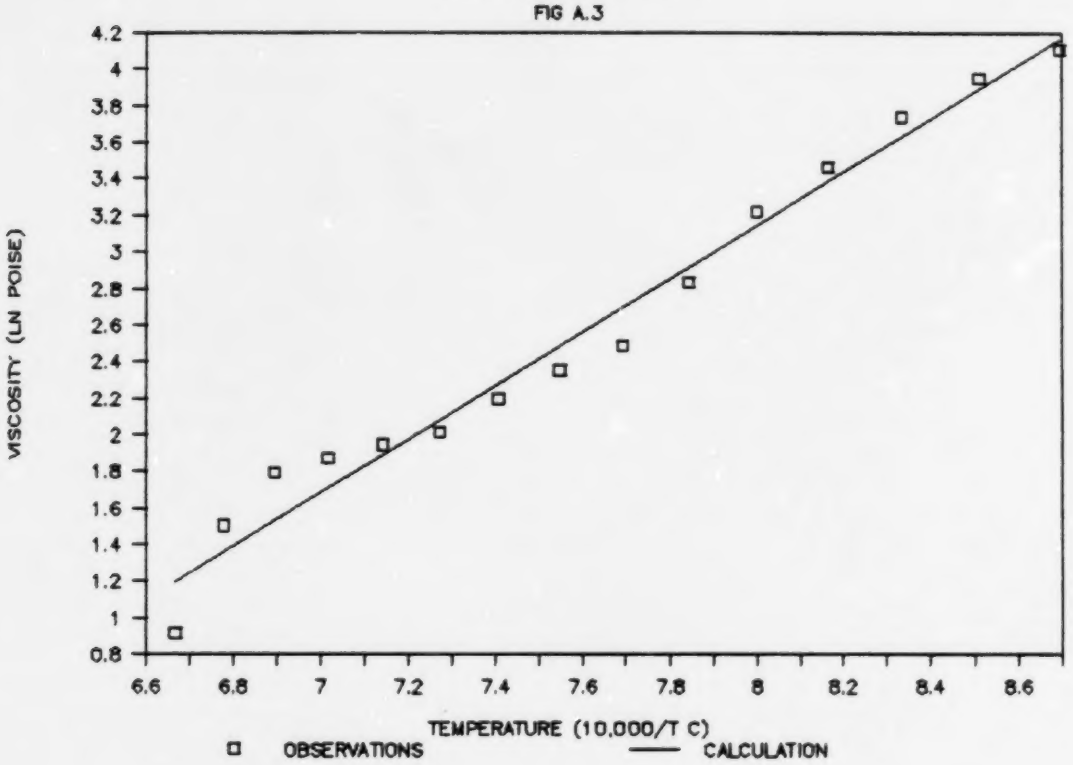

DAVIS' FLUX F3

TABLE A.3

TEMP	POISE	10000/T	LN(VISC)	CALC LN V
1500	2.5	6.666666	0.916290	1.198689
1475	4.5	6.779661	1.504077	1.363829
1450	6	6.896551	1.791759	1.534665
1425	6.5	7.017543	1.871802	1.711494
1400	7	7.142857	1.945910	1.894639
1375	7.5	7.272727	2.014903	2.084444
1350	9	7.407407	2.197224	2.281279
1325	10.5	7.547169	2.351375	2.485541
1300	12	7.692307	2.484906	2.697659
1275	17	7.843137	2.833213	2.918096
1250	25	8	3.218875	3.147351
1225	32	8.163265	3.465735	3.385962
1200	42	8.333333	3.737669	3.634516
1175	52	8.510638	3.951243	3.893647
1150	61	8.695652	4.110873	4.164044

Regression Output:

Constant	-8.54462
Std Err of Y Est	0.153040
R Squared	0.976198
No. of Observations	15
Degrees of Freedom	13
X Coefficient(s)	1.461496
Std Err of Coef.	0.063293

DAVIS' FLUX F4

FIGURE A.4

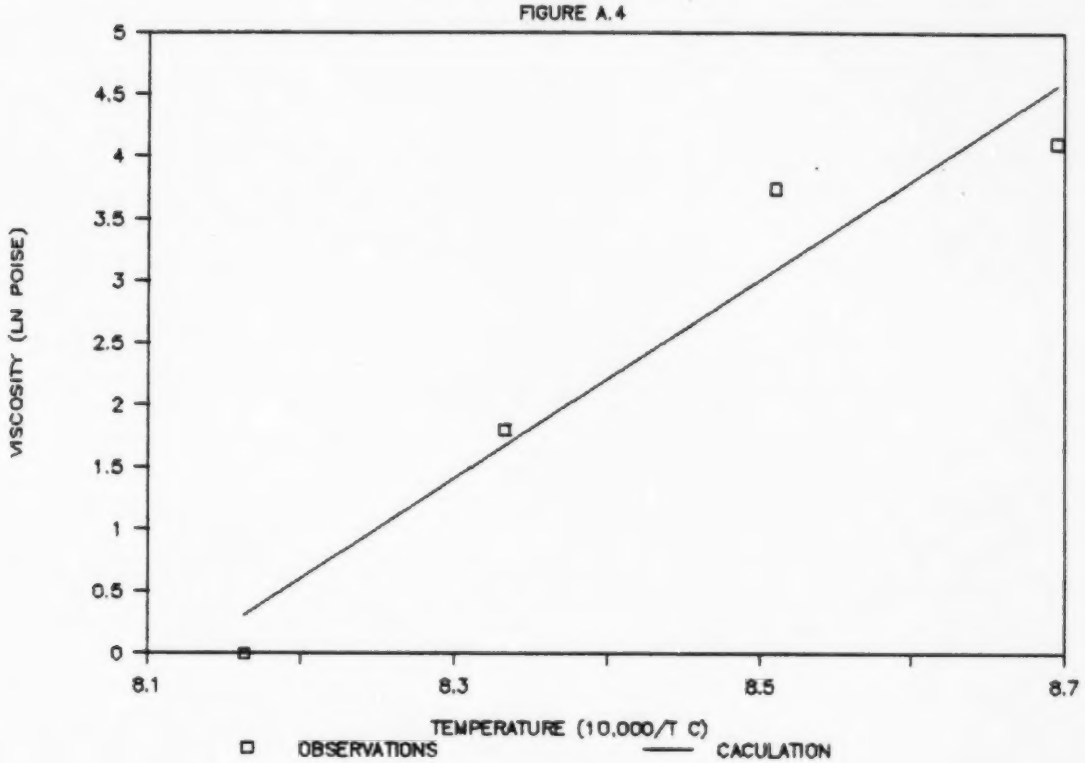

DAVIS' F4 FLUX

TABLE A.4

TEMP	POISE	10000/T	LN VISC	CALC LN VISC
1150	61	8.695652	4.110873	4.572186
1175	42	8.510638	3.737669	3.090244
1200	6	8.333333	1.791759	1.670049
1225	1	8.163265	0	0.307822

Regression Output:

Constant	-65.0791
Std Err of Y Est	0.608907
R Squared	0.931630
No. of Observations	4
Degrees of Freedom	2
X Coefficient(s)	8.009898
Std Err of Coef.	1.534340

DAVIS' FLUX F5

FIGURE A.5

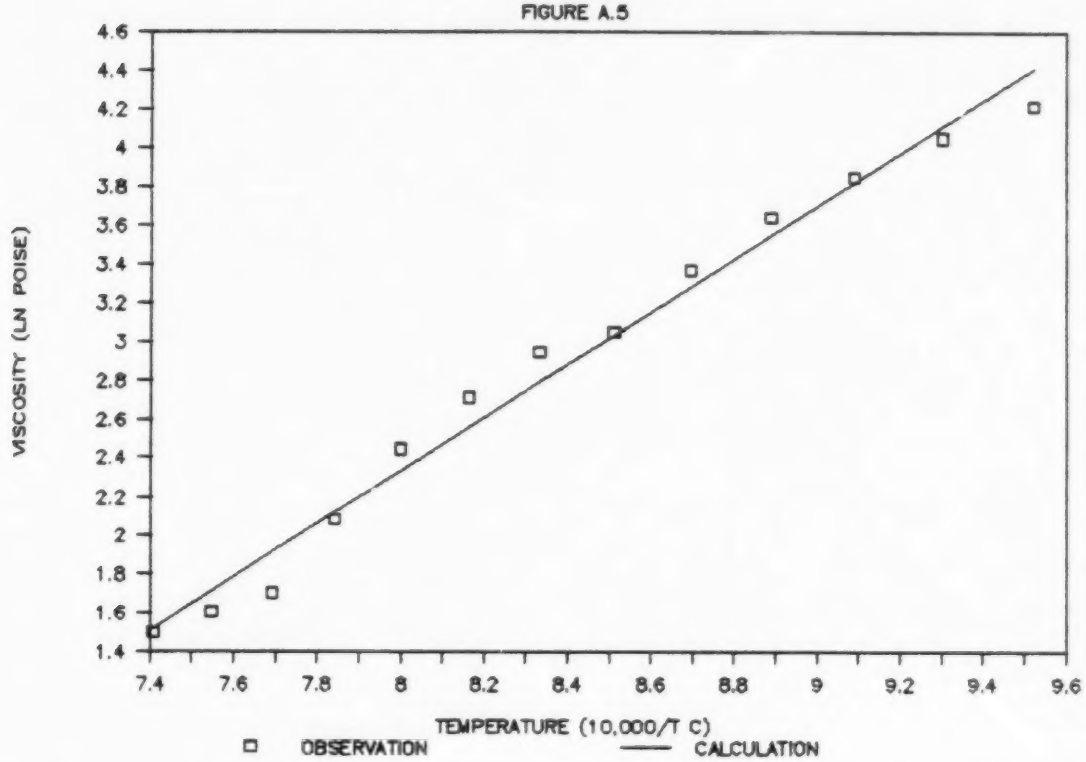

DAVIS'F5 FLUX

TABLE A.5

TEMP	POISE	I/TEMP	LN VISC	CALC LN VISC
1350	4.5	7.407407	1.504077	1.523359
1325	5	7.547169	1.609437	1.714363
1300	5.5	7.692307	1.704748	1.912713
1275	8	7.843137	2.079441	2.118842
1250	11.5	8	2.442347	2.333215
1225	15	8.163265	2.708050	2.556339
1200	19	8.333333	2.944438	2.788759
1175	21	8.510638	3.044522	3.031070
1150	29	8.695652	3.367295	3.283916
1125	38	8.888888	3.637586	3.547999
1100	47	9.090909	3.850147	3.824087
1075	57.5	9.302325	4.051784	4.113015
1050	68	9.523809	4.219507	4.415702

Regression Output:

Constant	-8.59984
Std Err of Y Est	0.125562
R Squared	0.983785
No. of Observations	13
Degrees of Freedom	11
X Coefficient(s)	1.366632
Std Err of Coef.	0.052899

DAVIS' FLUX F6

FIGURE A.6

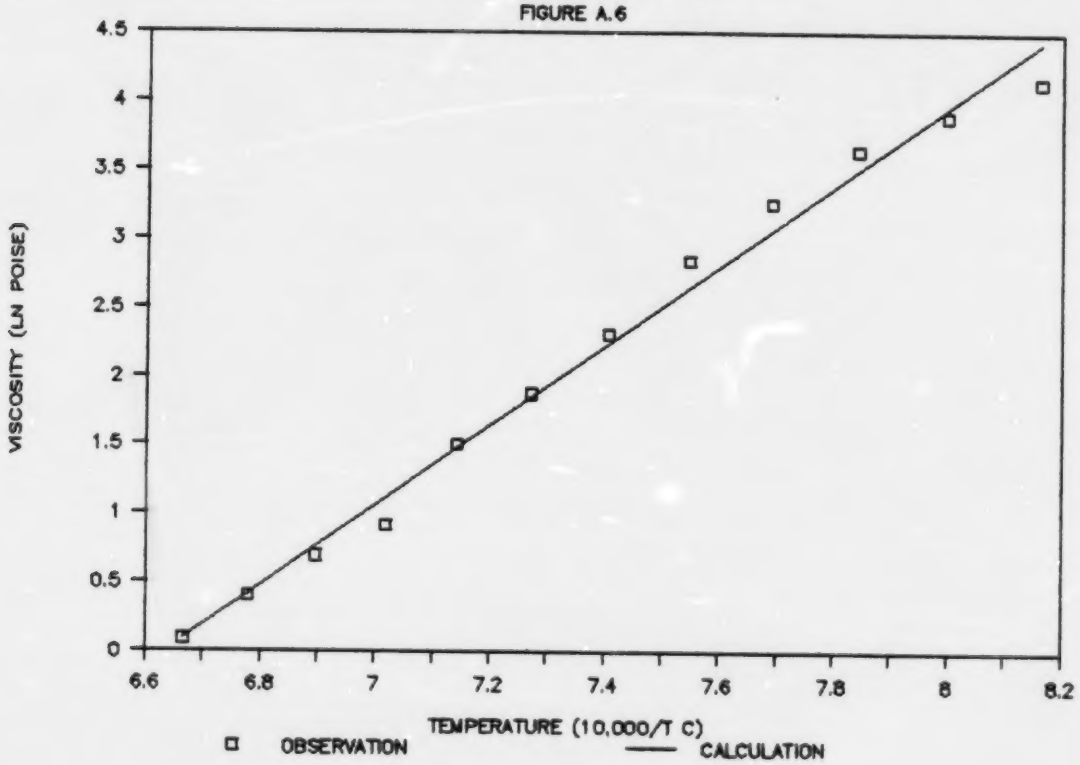

DAVIS' F6 FLUX

TABLE A.6

TEMP	POISE	10000/T	LN(VISC)	CALC LN VISC
1500	1.1	6.666666	0.095310	0.096205
1475	1.5	6.779661	0.405465	0.423260
1450	2	6.896551	0.693147	0.761593
1425	2.5	7.017543	0.916290	1.111797
1400	4.5	7.142857	1.504077	1.474508
1375	6.5	7.272727	1.871802	1.850409
1350	10	7.407407	2.302585	2.240232
1325	17	7.547169	2.833213	2.644766
1300	26	7.692307	3.258096	3.064858
1275	38	7.843137	3.637586	3.501425
1250	49	8	3.891820	3.955454
1225	63	8.163265	4.143134	4.428015

Regression Output:

Constant	-19.2000
Std Err of Y Est	0.150014
R Squared	0.989924
No. of Observations	12
Degrees of Freedom	10
X Coefficient(s)	2.894436
Std Err of Coef.	0.092339

DAVIS' FLUX F7

FIGURE A.7

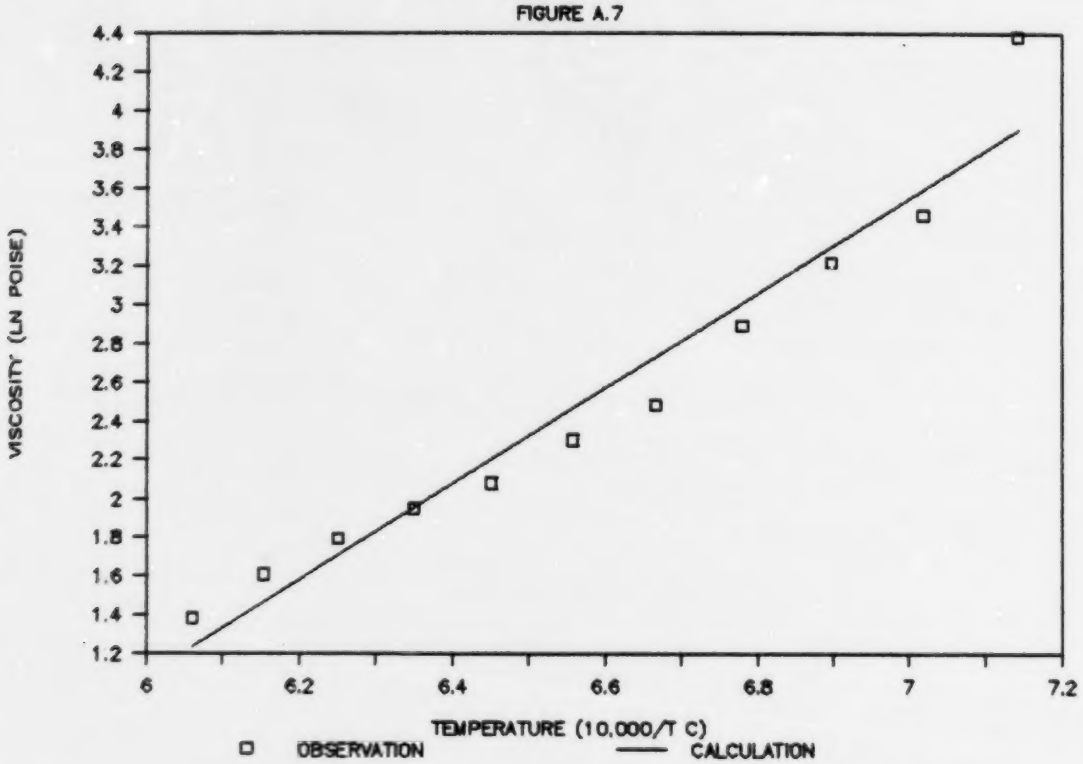

DAVIS' FLUX F8

DAVIS' F7 FLUX

TABLE A.7

TEMP	POISE	10000/T	LN VISC	CALC LN VISC
1650	4	6.060606	1.386294	1.239376
1625	5	6.153846	1.609437	1.468786
1600	6	6.25	1.791759	1.705366
1575	7	6.349206	1.945910	1.949456
1550	8	6.451612	2.079441	2.201420
1525	10	6.557377	2.302585	2.461645
1500	12	6.666666	2.484906	2.730544
1475	18	6.779661	2.890371	3.008559
1450	25	6.896551	3.218875	3.296160
1425	32	7.017543	3.465735	3.593852
1400	80	7.142857	4.382026	3.902176

Regression Output:

Constant	-13.6723
Std Err of Y Est	0.214986
R Squared	0.949282
No. of Observations	11
Degrees of Freedom	9
X Coefficient(s)	2.460427
Std Err of Coef.	0.189571

DAVIS' FLUX F8

FIGURE A.8

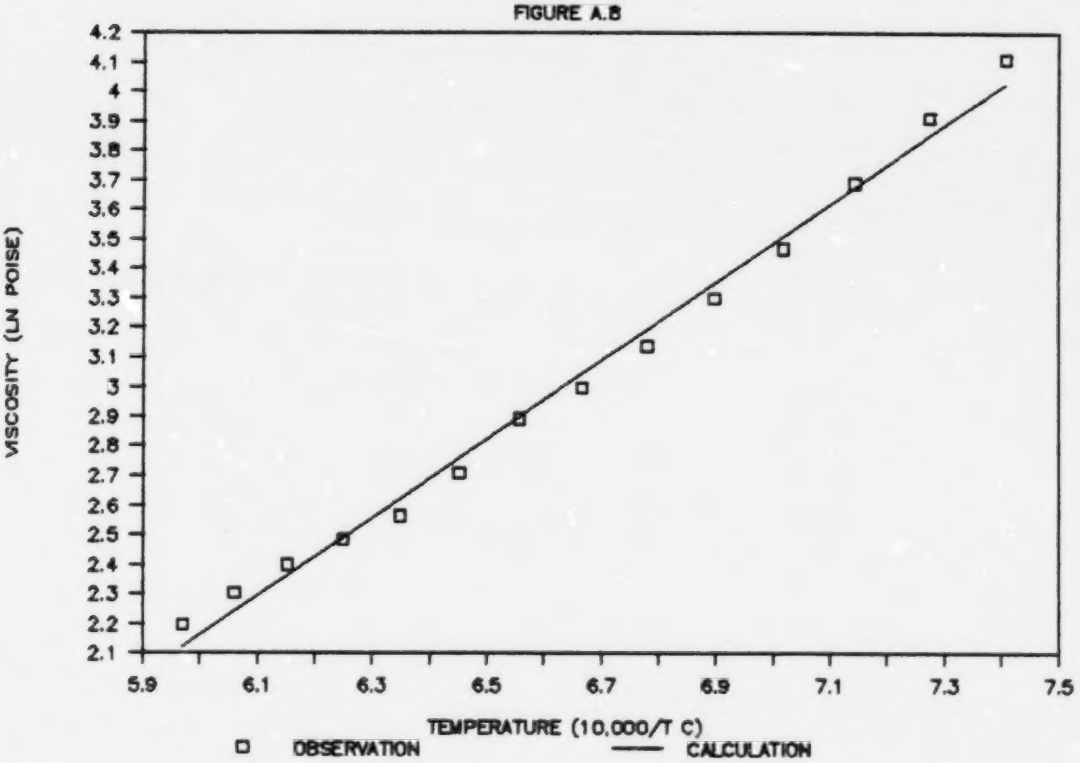

DAVIS' F8 FLUX

TABLE A.8

TEMP	POISE	10000/T	LN VISC	CALC LN VISC
1675	9	5.970149	2.197224	2.121294
1650	10	6.060606	2.302585	2.241200
1625	11	6.153846	2.397895	2.364795
1600	12	6.25	2.484906	2.492252
1575	13	6.349206	2.564949	2.623755
1550	15	6.451612	2.708050	2.759501
1525	18	6.557377	2.890371	2.899697
1500	20	6.666666	2.995732	3.044567
1475	23	6.779661	3.135494	3.194347
1450	27	6.896551	3.295836	3.349292
1425	32	7.017543	3.465735	3.509674
1400	40	7.142857	3.688879	3.675784
1375	50	7.272727	3.912023	3.847934
1350	61	7.407407	4.110873	4.026460

Regression Output:

Constant	-5.79246
Std Err of Y Est	0.056947
R Squared	0.992068
No. of Observations	14
Degrees of Freedom	12
X Coefficient(s)	1.325555
Std Err of Coef.	0.034214

DAVIS' FLUX 9

FIGURE A.9

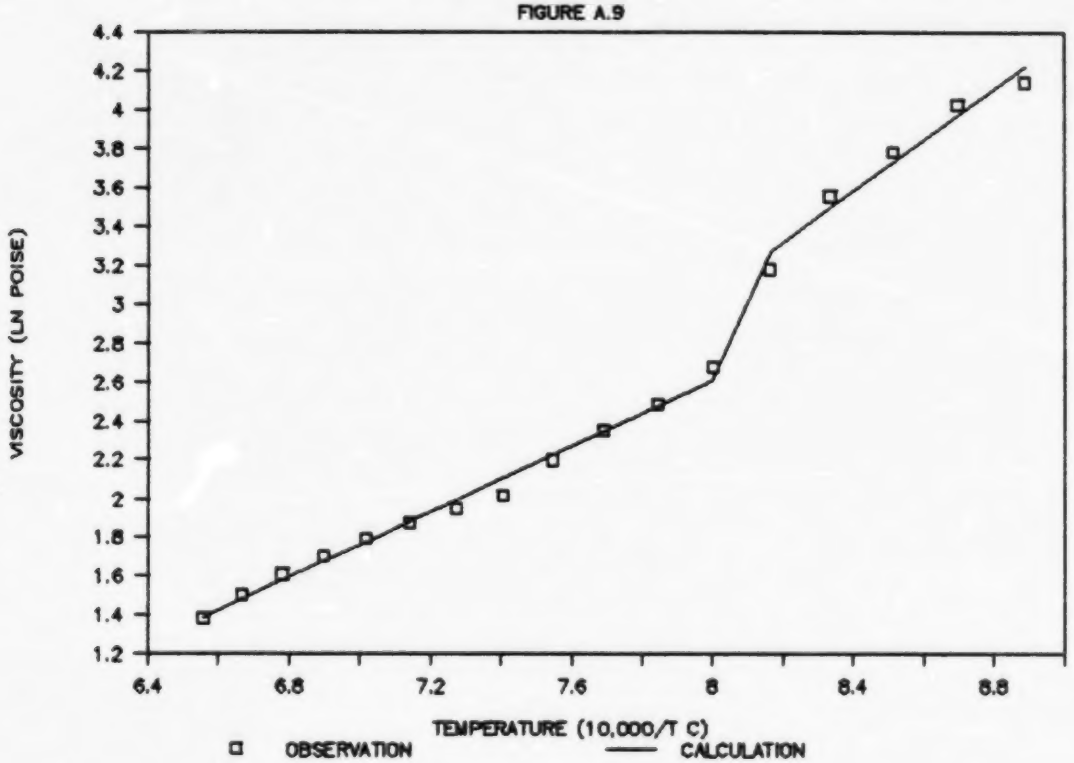

DAVIS' F9 FLUX

TABLE A.9

TEMP	POISE	10000/T	LN VISC	CALC LN VISC
1525	4	6.557377	1.386294	1.390309
1500	4.5	6.666666	1.504077	1.482375
1475	5	6.779661	1.609437	1.577562
1450	5.5	6.896551	1.704748	1.676032
1425	6	7.017543	1.791759	1.777956
1400	6.5	7.142857	1.871802	1.883521
1375	7	7.272727	1.945910	1.992924
1350	7.5	7.407407	2.014903	2.106380
1325	9	7.547169	2.197224	2.224116
1300	10.5	7.692307	2.351375	2.346381
1275	12	7.843137	2.484906	2.473441
1250	14.5	8	2.674148	2.605583
1225	24	8.163265	3.178053	3.269677
1200	35	8.333333	3.555348	3.493601
1175	44	8.510638	3.784189	3.727054
1150	56	8.695652	4.025351	3.970657
1125	63	8.888888	4.143134	4.225087

Regression Output:

Constant	-4.13366
Std Err of Y Est	0.043375
R Squared	0.989305
No. of Observations	12
Degrees of Freedom	10
X Coefficient(s)	0.842406
Std Err of Coef.	0.027697

Regression Output:

Constant	-7.47868
Std Err of Y Est	0.091614
R Squared	0.957733
No. of Observations	5
Degrees of Freedom	3
X Coefficient(s)	1.316674
Std Err of Coef.	0.159695

DAVIS' FLUX 10

FIGURE A.10

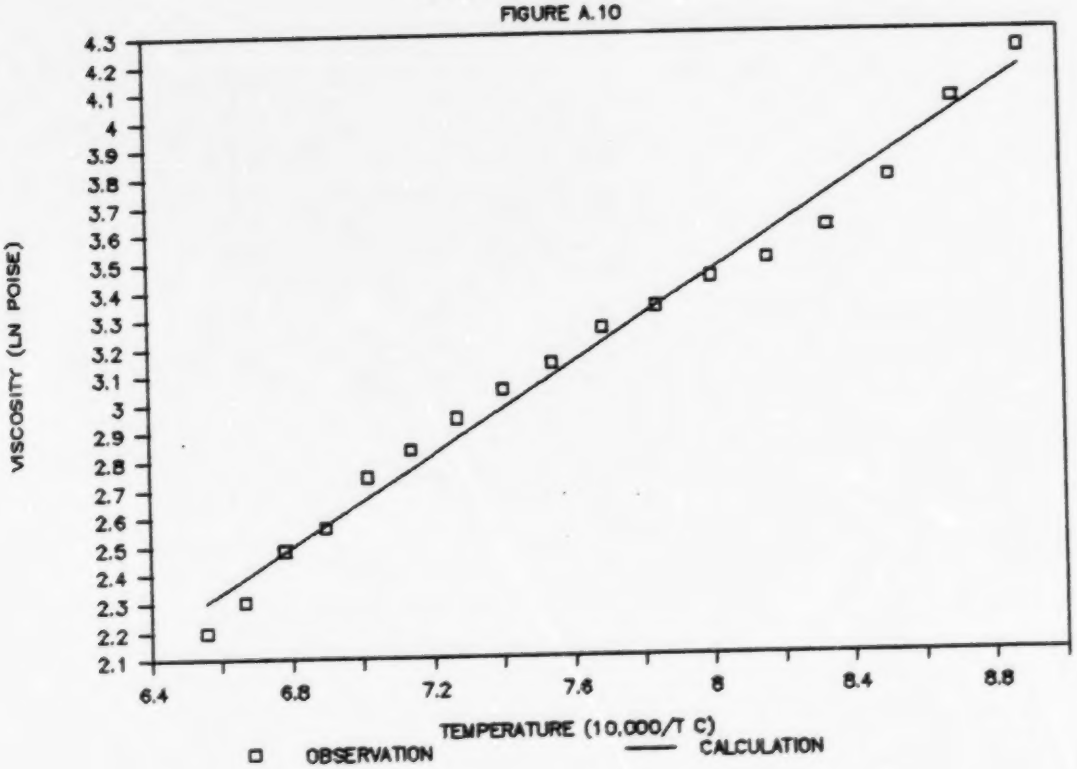

DAVIS' F10 FLUX

TABLE A.10

TEMP	POISE	10000/T	LN VISC	CALC LN VISC
1525	9	6.557377	2.197224	2.298703
1500	10	6.666666	2.302585	2.386310
1475	12	6.779661	2.484906	2.476887
1450	13	6.896551	2.564949	2.570588
1425	15.5	7.017543	2.740840	2.667576
1400	17	7.142857	2.833213	2.768028
1375	19	7.272727	2.944438	2.872133
1350	21	7.407407	3.044522	2.980094
1325	23	7.547169	3.135494	3.092129
1300	26	7.692307	3.258096	3.208473
1275	28	7.843137	3.332204	3.329379
1250	31	8	3.433987	3.455121
1225	33	8.163265	3.496507	3.585996
1200	37	8.333333	3.610917	3.722324
1175	44	8.510638	3.784189	3.864453
1150	58	8.695652	4.060443	4.012762
1125	69	8.888888	4.234106	4.167662

Regression Output:

Constant	-2.95774
Std Err of Y Est	0.070591
R Squared	0.986642
No. of Observations	17
Degrees of Freedom	15
X Coefficient(s)	0.801608
Std Err of Coef.	0.024082

EUTECTIC J (TUNS)

LOW SILICA FIGURE A.11

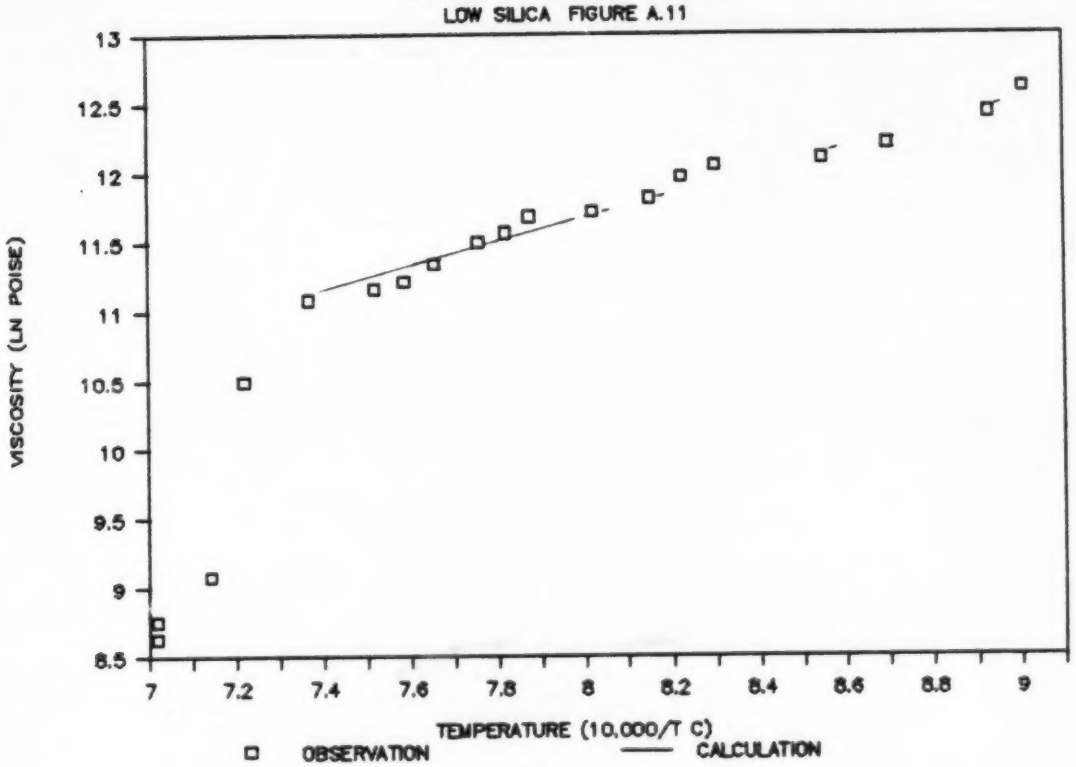

EUTECTIC J (TUNS)

TABLE A.11

%SiO2= 50
%TiO2= 15%Al2O3= 10
%CaO = 35

MELT TEMP = 1100 C

TEMP	POISE	10000/T	LN VISC	CALC LN VISC
1425	6400	7.017543	8.764053	8.637425
1425	5600	7.017543	8.630521	8.637425
1400	8800	7.142857	9.082507	9.534144
1385	36000	7.220216	10.49127	10.08771
1357	65000	7.369196	11.08214	11.15378
1330	70000	7.518796	11.15625	11.25037
1318	74000	7.587253	11.21182	11.31106
1306	84000	7.656967	11.33857	11.37287
1289	98000	7.757951	11.49272	11.46240
1279	105000	7.818608	11.56171	11.51617
1270	118000	7.874015	11.67843	11.56529
1247	122500	8.019246	11.71586	11.69404
1227	135000	8.149959	11.81303	11.80993
1216	157500	8.223684	11.96718	11.87529
1205	170000	8.298755	12.04355	11.94184
1170	180000	8.547008	12.10071	12.16193
1150	200000	8.695652	12.20607	12.29371
1120	250000	8.928571	12.42921	12.50020
1110	300000	9.009009	12.61153	12.57151

Regression Output:

Constant	4.584635
Std Err of Y Est	0.078009
R Squared	0.971277
No. of Observations	14
Degrees of Freedom	12
X Coefficient(s)	0.886543
Std Err of Coef.	0.044009

Regression Output:

Constant	-41.5788
Std Err of Y Est	0.359653
R Squared	0.920758
No. of Observations	5
Degrees of Freedom	3
X Coefficient(s)	7.155812
Std Err of Coef.	1.211995

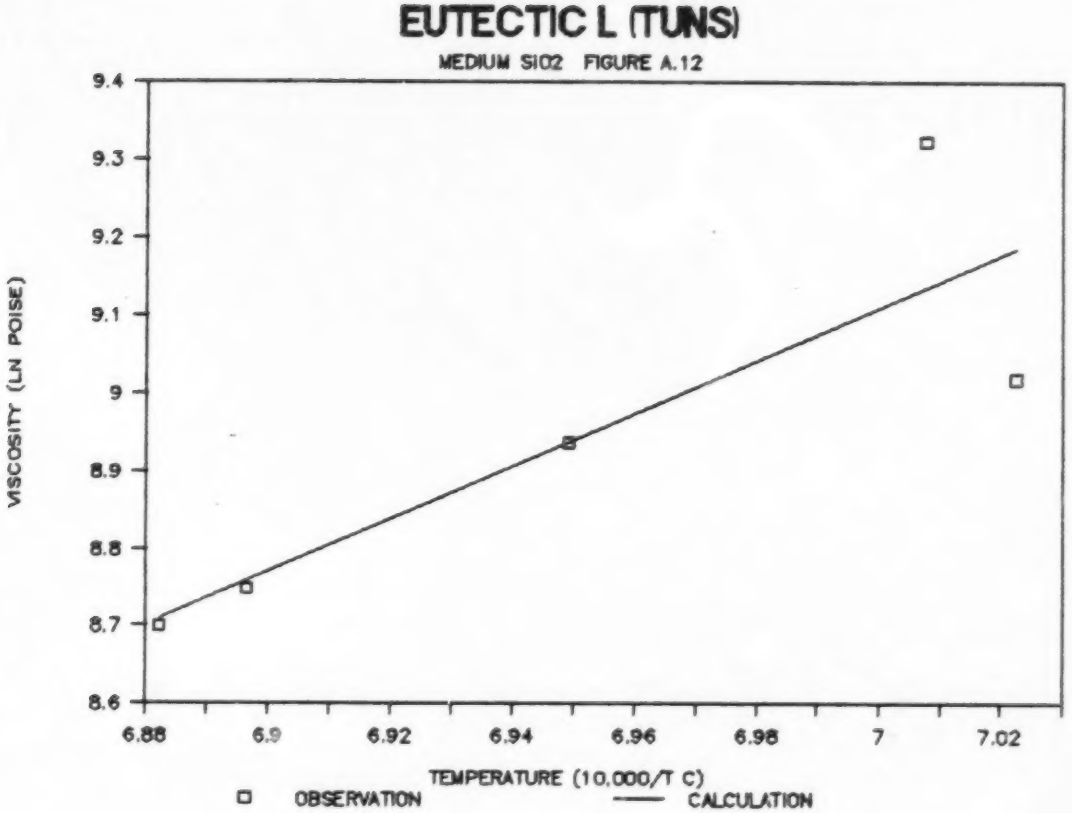
EUTECTIC L (TUNS)
MEDIUM SIO2 FIGURE A.12
VISCOSITY (LN POISE)
9.4
9.3
9.2
9.1
9
8.9
8.8
8.7
8.6
6.88
6.9
6.92
6.94
6.96
6.98
7
7.02
TEMPERATURE (10,000/T C)
OBSERVATION
CALCULATION

EUTECTIC L (TUNS)

TABLE A.12

%TiO2 = 50 MELT TEMP = 1338 C
%SiO2 = 30 %Al2O3=10
%CaO = 20

TEMP	POISE	10000/T	LN VISC	CALC LN VISC
1453	6000	6.882312	8.699514	8.709927
1450	6300	6.896551	8.748304	8.758208
1439	7600	6.949270	8.935903	8.936959
1427	11200	7.007708	9.323669	9.135103
1424	8250	7.022471	9.017968	9.185161

Regression Output:

Constant	-14.6256
Std Err of Y Est	0.145737
R Squared	0.742812
No. of Observations	5
Degrees of Freedom	3
X Coefficient(s)	3.390661
Std Err of Coef.	1.151885

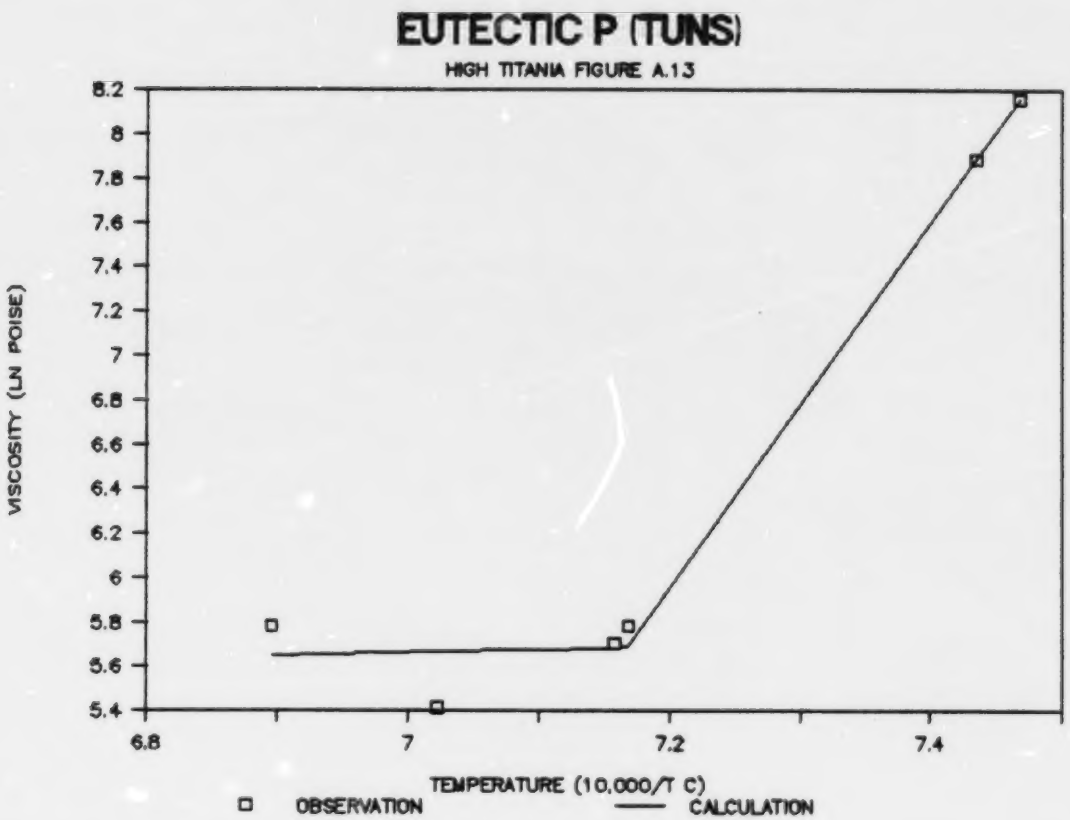
EUTECTIC P (TUNS)
HIGH TITANIA FIGURE A.13
VISCOSITY (LN POISE)
8.2
8
7.8
7.6
7.4
7.2
7
6.8
6.6
6.4
6.2
6
5.8
5.6
5.4
6.8
7
7.2
7.4
TEMPERATURE (10,000/T C)
OBSERVATION
CALCULATION

EUTECTIC P (TUNS)

TABLE A.13

%TiO2 = 57 MELT TEMP = 1310 C
%SiO2 = 18 %Al2O3= 10
%CaO = 25

TEMP	POISE	10000/T	LN VISC	CALC LN VISC
1450	325	6.896551	5.783825	5.649991
1424	225	7.022471	5.416100	5.666711
1397	300	7.158196	5.703782	5.684733
1395	325	7.168458	5.783825	5.686096
1345	2660	7.434944	7.886081	7.891850
1339	3500	7.468259	8.160518	8.155360

Regression Output:

Constant	4.734219
Std Err of Y Est	0.212874
R Squared	0.009542
No. of Observations	4
Degrees of Freedom	2
X Coefficient(s)	0.132786
Std Err of Coef.	0.956593

Regression Output:

Constant	-50.9148
Std Err of Y Est	0.005509
R Squared	0.999988
No. of Observations	4
Degrees of Freedom	2
X Coefficient(s)	7.909497
Std Err of Coef.	0.019042

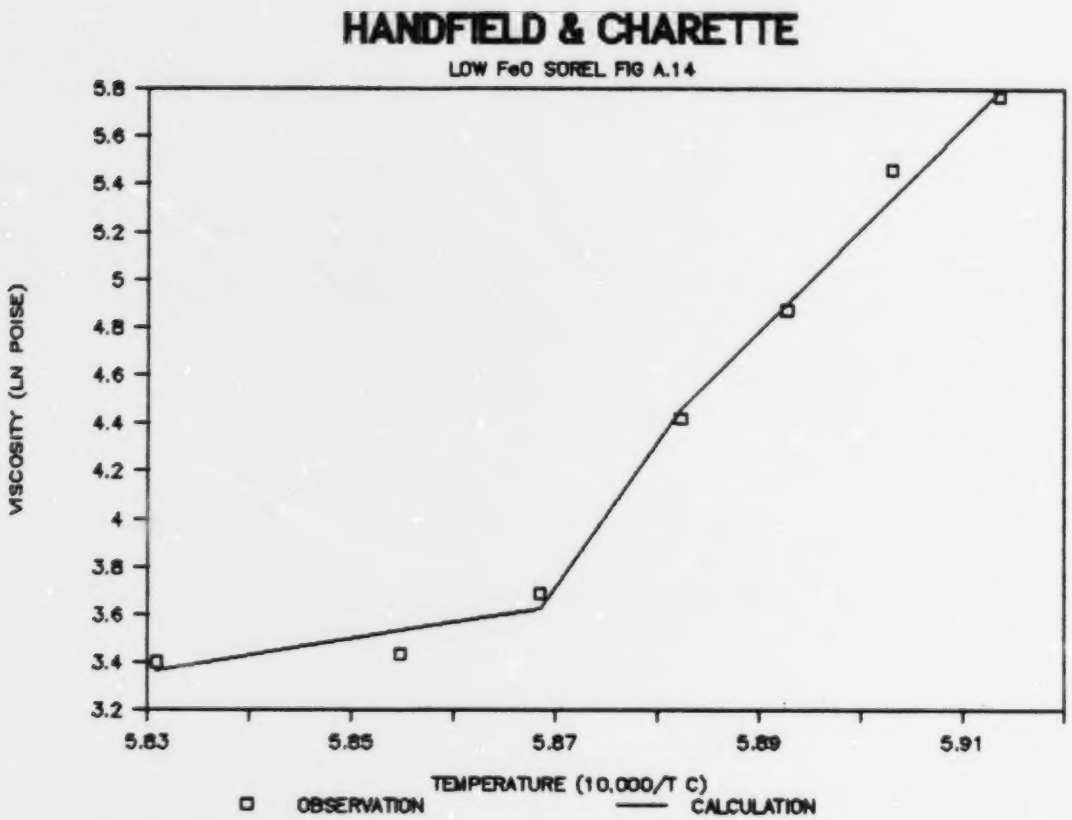
HANDFIELD & CHARETTE
LOW FeO SOREL FIG A.14
VISCOSITY (LN POISE)
5.8
5.6
5.4
5.2
5
4.8
4.6
4.4
4.2
4
3.8
3.6
3.4
3.2
5.83
5.85
5.87
5.89
5.91
TEMPERATURE (10,000/T C)
OBSERVATION
CALCULATION

HANDFIELD & CHARETTE
LOW FeO SOREL

TABLE A.14

TEMP	VISC	10000/T	LN VISC	CALC VISC
1715	30	5.830903	3.401197	3.365584
1708	31	5.854800	3.433987	3.531522
1704	40	5.868544	3.688879	3.626956
1700	83	5.882352	4.418840	4.456225
1697	130	5.892751	4.867534	4.897986
1694	235	5.903187	5.459585	5.341312
1691	320	5.913660	5.768320	5.786210
1689	>500			

Regression Output:

Constant	-245.433
Std Err of Y Est	0.133481
R Squared	0.983794
No. of Observations	6
Degrees of Freedom	4
X Coefficient(s)	42.48120
Std Err of Coef.	2.726150

Regression Output:

Constant	-37.1233
Std Err of Y Est	0.120896
R Squared	0.705337
No. of Observations	3
Degrees of Freedom	1
X Coefficient(s)	6.943850
Std Err of Coef.	4.488122

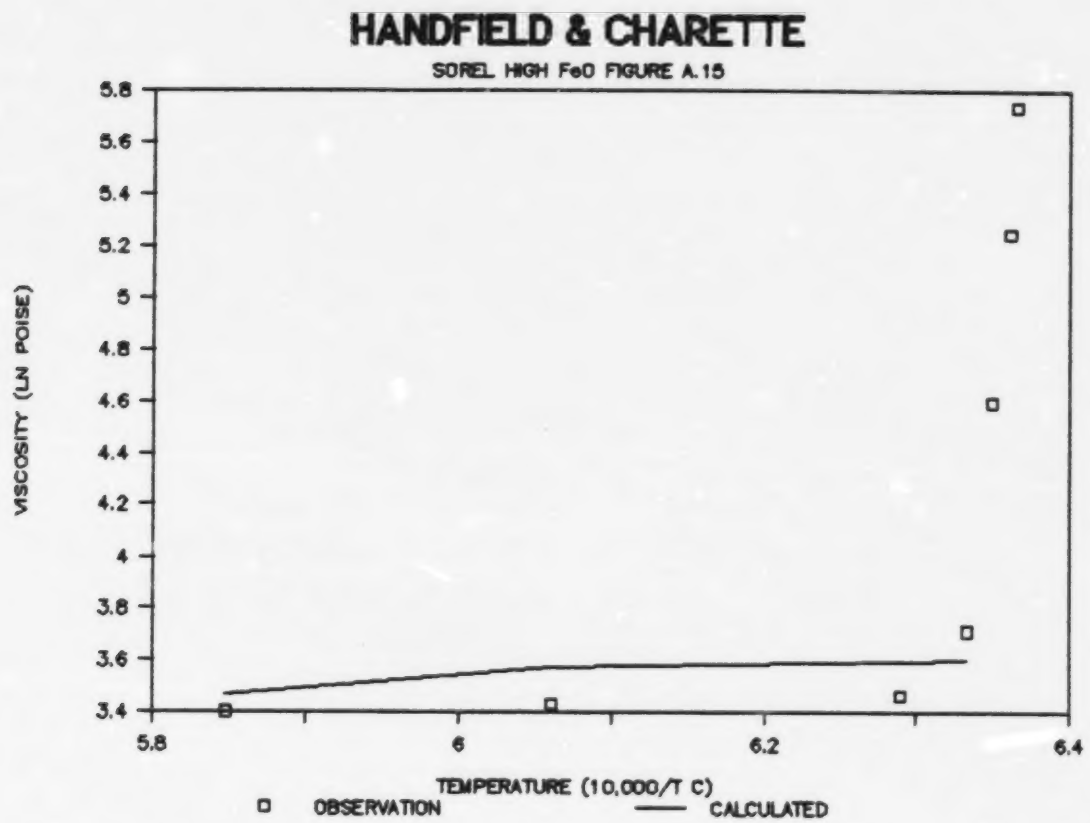
HANDFIELD & CHARETTE
SOREL HIGH FeO FIGURE A.15
VISCOSITY (LN POISE)
5.8
5.6
5.4
5.2
5
4.8
4.6
4.4
4.2
4
3.8
3.6
3.4
5.8
6
6.2
6.4
TEMPERATURE (10,000/T C)
OBSERVATION
CALCULATED

Handfield and Charette
HIGH FeO SOREL

TABLE A.15

TEMP	VISC	10000/T	LN VISC	CALC VISC
1710	30	5.847953	3.401197	3.470016
1650	31	6.060606	3.433987	3.576556
1590	32	6.289308	3.465735	3.596967
1579	41	6.333122	3.713572	3.604460
1575	99	6.349206	4.595119	5.372378
1572	190	6.361323	5.247024	5.642616
1571	310	6.365372	5.736572	5.913199
1570	>500	6.369426	ERR	

Regression Output:

Constant	0.646693
Std Err of Y Est	0.118513
R Squared	0.538392
No. of Observations	4
Degrees of Freedom	2
X Coefficient(s)	0.465848
Std Err of Coef.	0.305011

Regression Output:

Constant	-419.172
Std Err of Y Est	0.159772
R Squared	0.961077
No. of Observations	3
Degrees of Freedom	1
X Coefficient(s)	66.73842
Std Err of Coef.	13.43060

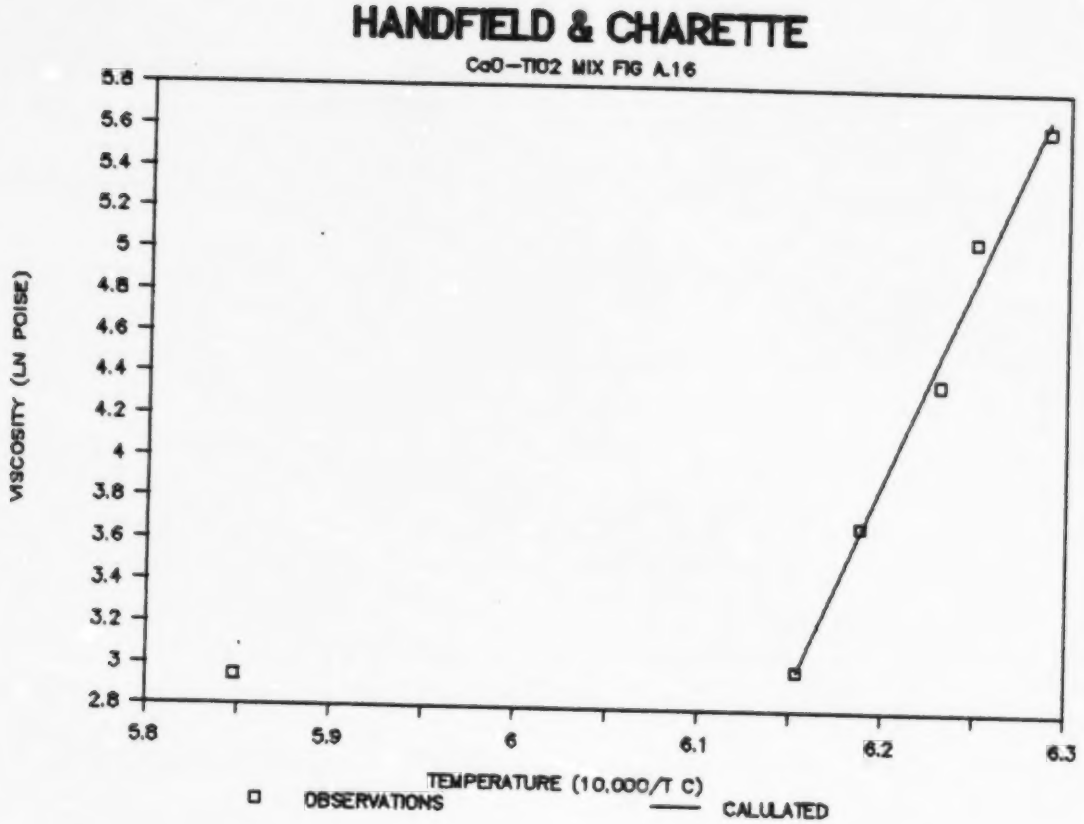
HANDFIELD & CHARETTE
CaO–TiO2 MIX FIG A.16
VISCOSITY (LN POISE)
5.8
5.6
5.4
5.2
5
4.8
4.6
4.4
4.2
4
3.8
3.6
3.4
3.2
3
2.8
5.8
5.9
6
6.1
6.2
6.3
TEMPERATURE (10,000/T C)
OBSERVATIONS
CALULATED

HANDFIELD & CHARETTE
CaO-TiO2 MIX

TABLE A.16

TEMP	VISC	10000/T	LN VISC	CALC VISC
1710	19	5.847953	2.944438	
1625	20	6.153846	2.995732	3.000123
1616	40	6.188118	3.688879	3.676225
1605	80	6.230529	4.382026	4.512868
1600	160	6.25	5.075173	4.896963
1590	275	6.289308	5.616771	5.672401
1578	>500			

Regression Output:

Constant	-118.397
Std Err of Y Est	0.131849
R Squared	0.988154
No. of Observations	5
Degrees of Freedom	3
X Coefficient(s)	19.72713
Std Err of Coef.	1.247005